

Relationship between the Mesoporous Intermediate Layer Structure and the Gas Permeation Property of an Amorphous Silica Membrane Synthesized by Counter Diffusion Chemical Vapor Deposition

Takayuki Nagano,[†] Shinji Fujisaki, Koji Sato, Koji Hataya, and Yuji Iwamoto

Japan Fine Ceramics Center, Nagoya 456-8587, Japan

Mikihiro Nomura

Shibaura Institute of Technology, Tokyo 135-8548, Japan

Shin-Ichi Nakao

University of Tokyo, Tokyo 113-8656, Japan

An amorphous silica membrane with an excellent hydrogen/nitrogen (H₂/N₂) permselectivity of >10 000 and a He/H₂ permselectivity of 11 was successfully synthesized on a γ -alumina (γ -Al₂O₃)-coated α -alumina (α -Al₂O₃) porous support by counter diffusion chemical vapor deposition using tetramethylorthosilicate and oxygen at 873 K. An amorphous silica membrane possessed a high H₂ permeance of $>1.0 \times 10^{-7}$ mol·(m²·s·Pa)⁻¹ at ≥ 773 K. The dominant permeation mechanism for He and H₂ at 373–873 K was activated diffusion. On the other hand, that for CO₂, Ar, and N₂ at 373–673 K was a viscous flow. At ≥ 673 K, that for CO₂, Ar, and N₂ was activated diffusion. H₂ permselectivity was markedly affected by the permeation temperature, thickness, and pore size of a γ -Al₂O₃ mesoporous intermediate layer.

I. Introduction

HYDROGEN (H₂) has been attracting considerable attention as a clean alternative energy source for fossil hydrocarbon fuels. It is expected that H₂ will be produced using natural energies. However, it is difficult to meet the demand for H₂, and H₂ production through natural gas reforming has been investigated. For example, methane (CH₄), the main constituent of natural gas, is converted to H₂ and carbon monoxide (CO) through steam reforming as follows:



This reaction is endothermic and is induced at approximately 1073 K. In this process, the synthesis gas then proceeds to a water–gas shift reactor where steam and CO can be converted into H₂ and carbon dioxide (CO₂). Finally, H₂ is separated from the gas mixture using one of several adsorption technologies, such as pressure swing adsorption. Owing to a high operation temperature and several complex purification steps, the cost of producing H₂ with these current technologies is too high for it to be used as an alternative source for conventional hydrocarbon fuels. Therefore, decreasing the operation temperature and com-

binning these processes into a single step represent technical problems.^{1–3}

A membrane reactor has been investigated as a device for H₂ mass production. It is well known that the application of high-temperature membrane reactors to this steam-reforming step has the potential of achieving the same conversion efficiencies as those attained using conventional reactors at a significantly low temperature of approximately 773 K. If a membrane with a high durability under a steam atmosphere at elevated temperatures is developed, these technical problems can be solved concurrently. A palladium-based membrane with a high H₂ permselectivity is a candidate membrane reactor. However, there are some problems associated with the total cost of a resource.

An inorganic membrane with a high strength at elevated temperatures and a high chemical stability is used under a high pressure and corrosion atmosphere at elevated temperatures. Therefore, H₂ production processes can be combined to suppress energy loss. An amorphous silica membrane is well known as a H₂-permselective membrane. Amorphous silica membranes are produced by sol–gel coating,^{4,5} chemical vapor deposition (CVD) and chemical vapor infiltration (CVI),^{6–14} and precursor polymer pyrolysis.^{15,16} In CVD and CVI, the surfaces of large pores tend to be preferentially modified. Therefore, controlling the formation of pinhole defects is easy, and a high H₂ permeance to nitrogen (N₂) (H₂/N₂ permselectivity) has been reported in membranes synthesized by CVD and CVI. For example, Tsapatsis *et al.*⁸ oxidized SiCl₄ gas on porous Vycor glass by supplying H₂O gas and reported a H₂/N₂ permselectivity of 5000 at 723 K. Nijjimeijer *et al.*¹² prepared a microporous silica membrane on a mesoporous γ -alumina (γ -Al₂O₃)-coated α -alumina (α -Al₂O₃) porous support by low-temperature CVI and reported a H₂/N₂ permselectivity of >40 at 523 K. Hwang *et al.*¹³ prepared amorphous silica on α -Al₂O₃ porous tubes by CVD using tetraethylorthosilicate and reported a H₂/N₂ permselectivity of 160 at 873 K. Nomura *et al.*¹⁴ reported that a stable amorphous silica membrane synthesized by counter diffusion chemical vapor deposition (CDCVD) showed a H₂/N₂ permselectivity of >1000.

Inorganic membranes are composed of an active layer for separating gas, an intermediate layer for suppressing the formation of pinhole defects on the active layer, and a porous support. In the preparation of a microporous membrane by CVD and CVI, the gas separation property strongly depends on the structure of the mesoporous intermediate layer. However, the relationship between the intermediate layer structure and gas separation property has been reported in only a few papers. Hwang *et al.*¹³ synthesized amorphous silica membranes on α -Al₂O₃ with an average pore size of 100 nm and γ -Al₂O₃

T. Bessmann—contributing editor

Manuscript No. 23078. Received April 13, 2007; approved August 14, 2007. This work was carried out as a part of the R&D Project on “Highly Efficient Ceramic Membranes for High-Temperature Separation of Hydrogen” supported by the New Energy and Industrial Technology Development Organization (NEDO), Japan.

[†]Author to whom correspondence should be addressed. e-mail: t_nagano@jfcc.or.jp

(average pore size of 10 nm)-coated α -Al₂O₃. They reported that He permeance and He/N₂ permselectivity in amorphous silica on γ -Al₂O₃-coated α -Al₂O₃ were higher than those in amorphous silica on α -Al₂O₃. Nomura *et al.*¹⁷ synthesized amorphous silica membranes on γ -Al₂O₃ (average pore sizes of 4 and 13 nm)-coated α -Al₂O₃ by CDCVD. They reported that H₂ permeance and H₂/N₂ permselectivity in amorphous silica on γ -Al₂O₃ (4 nm)-coated α -Al₂O₃ were higher than those in amorphous silica on γ -Al₂O₃ (13 nm)-coated α -Al₂O₃.

To obtain a high H₂ permeance, the active layer should have a large path area and a small thickness. However, the large pore size of the intermediate layer leads to a pinhole defect and large thickness of the active layer. On the other hand, to obtain high H₂/N₂ permselectivity, the pore surface of the intermediate layer should be modified within the kinetic diameter of N₂. H₂ can permeate an amorphous silica network. Therefore, even if the pore of the intermediate layer is completely plugged with amorphous silica, high H₂ permselectivity can be expected.

In CDCVD, a membrane is synthesized at the contact point of the source and reaction gases inside the intermediate layer, as shown in Fig. 1. The pore size, pore filling homogeneity, silica density gradient of the intermediate layer, and effective membrane thickness can be controlled by changing the reactants and reaction conditions. The deposition rate of the membrane automatically decreases when the diffusion rates of the source and reaction gases decrease with the deposition. Therefore, the amorphous silica membrane synthesized by CDCVD exhibits a high H₂ permeance.

In this study, we investigated the relationships among the gas separation property, pore size, and thickness of a γ -Al₂O₃ mesoporous intermediate layer in an amorphous silica membrane on γ -Al₂O₃-coated α -Al₂O₃ synthesized by CDCVD.

II. Experimental Procedure

An α -Al₂O₃ porous capillary tube (150 nm in mean pore diameter, 2.9 mm in outer diameter, 2.1 mm in inner diameter, 400 mm in length, NOK Corporation, Tokyo, Japan) was used as a substrate. An effective membrane area with a length of 5 cm was at the center of the substrate. The dip-coating solution for γ -Al₂O₃ was obtained by diluting boehmite sol (γ -AlOOH) with a 3.5 wt% solution of polyvinyl alcohol (mean molecular weight = 72 000; Kanto Kagaku Co. Ltd., Tokyo, Japan) at 363 K. The end of the α -Al₂O₃ substrate was plugged. The outer surface of the substrate was dipped in the solution for 10 s, whereas the inner surface of the capillary was evacuated to obtain a pinhole-free membrane using a vacuum pump. After dipping, the membrane was dried for 2 h in air. It was then calcined at 873 or 1073 K for 1 h at a heating/cooling rate of 1 K/min. This dipping–drying–firing sequence was repeated once or twice. The γ -Al₂O₃-coated α -Al₂O₃ substrates prepared are shown in Table I.

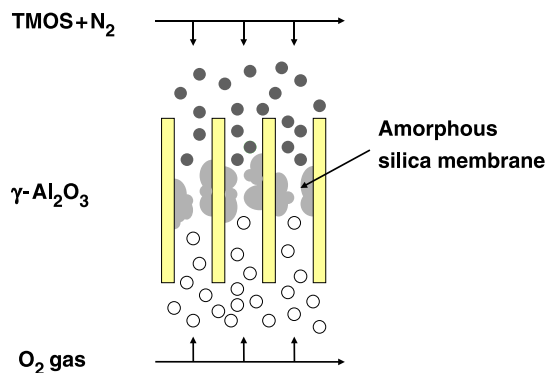


Fig. 1. Formation mechanism of gas separation membrane in counter diffusion chemical vapor deposition.

Table I. Preparation Conditions of γ -Al₂O₃-Coated α -Al₂O₃ Capillaries

Sample	Number of γ -Al ₂ O ₃ coatings	Calcination temperatures
1A	1	873 K 1 h
2A	2	873 K 1 h
1B	1	1073 K 1 h
2B	2	1073 K 1 h

The pore size distribution of the γ -Al₂O₃ intermediate layer on the α -Al₂O₃ substrate was analyzed using a nanoporometer (TNF-3WH-110ME; Seika Sangyo Co., Tokyo, Japan). N₂ was used as a noncondensable gas, and the liquid used as condensable vapor was water. Specimens were placed in the apparatus after annealing at 393 K for 1 h.

The amorphous silica coating of a γ -Al₂O₃-coated α -Al₂O₃ substrate was performed by CDCVD, as shown in Fig. 2. The substrate was coaxially fixed in a stainless tube and placed in an electric tubular furnace. Tetramethylorthosilicate was supplied through the outer surface of the substrate by controlling the N₂ flow rate at 200 mL/min. Oxygen (O₂) was introduced into the inner surface of the substrate at a flow rate of 200 mL/min. The substrate temperature and deposition time were 873 K and 1 h, respectively.

The top surfaces and cross-sectional structure of γ -Al₂O₃-coated α -Al₂O₃ capillaries were observed by scanning electron microscopy (SEM; Model S-4500, Hitachi, Tokyo, Japan).

Transmission electron microscopy (TEM) specimens were prepared using a focused ion beam (FIB) system (Model FB-2100, Hitachi) at acceleration voltages of 40–10 kV. Tungsten was deposited on the surface of the sampling area in the FIB system to protect the top layer of the membrane from gallium ion sputtering during FIB milling. The membrane was dug out by FIB milling and small specimens (3 μ m \times 25 μ m \times 15 μ m) were prepared. The specimens were lifted out using a tungsten needle and transferred to TEM grids. The specimens were then fixed onto the TEM grids by FIB-assisted deposition and thinned by FIB milling.

The cross-sectional structure of a silica membrane on a γ -Al₂O₃-coated α -Al₂O₃ capillary was observed by 200 kV TEM (Model EM002B, TOPCON, Tokyo, Japan). The specimen surface was coated with carbon to prevent charge-up during TEM observation. The composition of the top layer was analyzed by energy-dispersive X-ray spectroscopy (EDS) with TEM.

Single gas permeance (P) was evaluated by a constant-volume manometric method. Permeance data can be measured from 1×10^{-5} to 1×10^{-12} mol \cdot (m² \cdot s \cdot Pa)⁻¹ by varying the experimental conditions. The outside of the membrane was filled with pure gas under atmospheric pressure conditions. The inside of the membrane was evacuated using a vacuum pump. After terminating evacuation, the rate of pressure increase inside the membrane was measured five times to calculate permeance. The

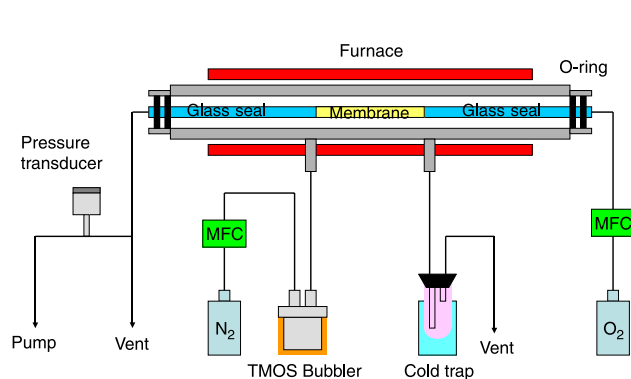


Fig. 2. Schematic illustration of counter diffusion chemical vapor deposition.

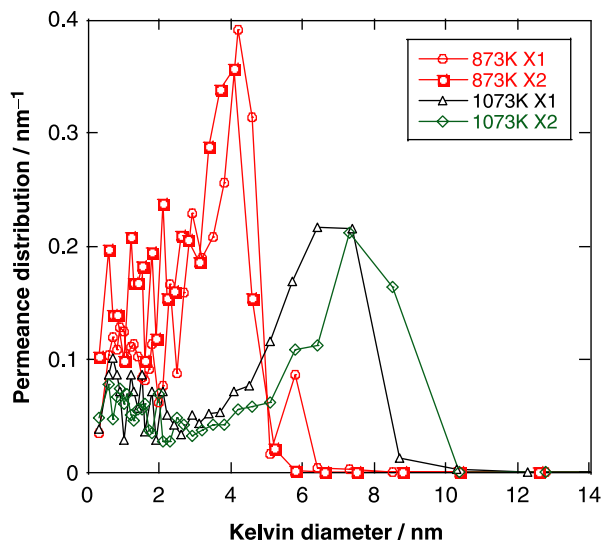


Fig. 3. Pore size distributions of γ - Al_2O_3 calcined at 873 and 1073 K for 1 h.

average of the third, fourth, and fifth measurements was accepted as permeance data. The gas permeance at each temperature was evaluated in the order of He, H_2 , CO_2 , Ar, and N_2 . Permselectivity was defined as the permeance ratio of the two gases. For example, the H_2/N_2 permselectivity is given by the ratio $P_{\text{H}_2}/P_{\text{N}_2}$.

III. Results and Discussion

(1) Microstructure of Amorphous Silica Membrane

The effect of calcination temperature on the pore size distribution of the γ - Al_2O_3 intermediate layer is shown in Fig. 3. The pore sizes of the sample calcined at 873 K for 1 h were almost entirely distributed between 2 and 5 nm. On the other hand, the pore sizes of the sample calcined at 1073 K for 1 h were almost distributed between 4 and 10 nm. The average pore sizes of the specimens increased with calcination temperature. The pore size distribution did not depend on the number of coatings. The average pore sizes of the specimens calcined at 873 and 1073 K were 3.6–4.0 and 6.6–7.6 nm, respectively.

The SEM top surface image and cross-sectional image of the γ - Al_2O_3 -coated α - Al_2O_3 capillary are shown in Figs. 4 and 5. Pinholes and cracks were not observed on the specimen surface. The surface morphology did not change with calcination temperature and the number of coatings. α - Al_2O_3 was uniformly coated with the γ - Al_2O_3 layers, and the thicknesses of the γ - Al_2O_3 layers in Samples 1A, 2A, 1B, and 2B were approximately 1.8, 2.6, 2.0, and 3.0 μm , respectively.

The TEM cross-sectional images and diffraction patterns of the synthesized sample of amorphous silica on Sample 2B are shown in Fig. 6. The top layer was observed as a defect-free thin layer having a thickness of approximately 2.3 μm . The thickness of the top layer was almost equal to that of the γ - Al_2O_3 intermediate layer, as shown in Fig. 5. The selected area diffraction patterns of the top layer were identical to those of amorphous silica and γ - Al_2O_3 . The diffuse ring patterns were assigned to γ - Al_2O_3 , suggesting that each grain was less crystalline γ - Al_2O_3 . The TEM sample was also analyzed by EDS. EDS showed that the entire top layer was composed of silicon (Si), aluminum (Al), and O_2 .

The Si/Al atomic ratios of the γ - Al_2O_3 layer for amorphous silica on Sample 2B are shown in Fig. 7. The x-axis (distance from the surface) is zero, indicating the surface of the γ - Al_2O_3 shown in Fig. 6. The Si/Al ratios near the surface (distance from membrane surface approximately $<0.18 \mu\text{m}$) of the γ - Al_2O_3 layer were increased sharply. The effective membrane thickness

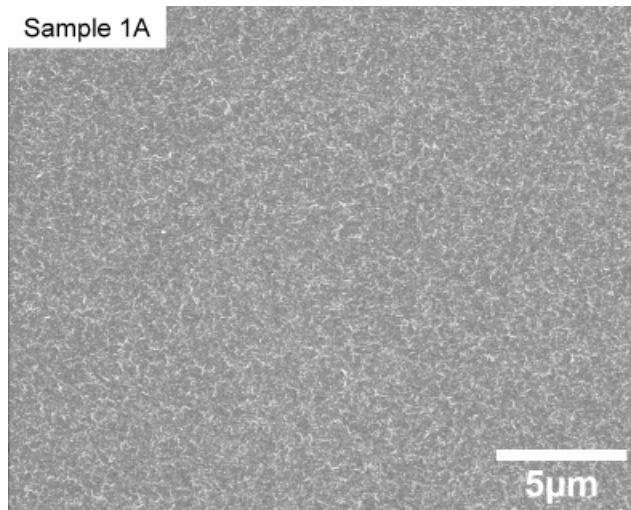


Fig. 4. Scanning electron microscopic top surface image of Sample 1A.

for gas separation was estimated to be 1/13 of the γ - Al_2O_3 layer thickness.

Therefore, the synthesized sample was considered to be composed of two layers, namely, an α - Al_2O_3 porous support and a γ - Al_2O_3 intermediate layer gradually modified with amorphous silica.

(2) Gas Permeation Property

The gas permeation behavior of the γ - Al_2O_3 intermediate layer on the α - Al_2O_3 porous capillaries is shown in Fig. 8. The experimental data at 873 K were plotted versus the square root of molecular weight. The gas permeance of Sample 1B with an average pore size of 7.6 nm was higher than that of Sample 1A with an average pore size of 4 nm. The permeance order of the gases through a γ - Al_2O_3 -coated α - Al_2O_3 capillary was $\text{H}_2 > \text{He} > \text{N}_2 > \text{Ar} > \text{CO}_2$. The linear regression fit is presented in Fig. 8. The results show a good linear dependence, confirming that the transport of the gases is induced mainly by Knudsen diffusion. The H_2 permselectivities over the other gases (Sample 1A: He: 1.38, CO_2 : 4.47, Ar: 4.09, N_2 : 3.39; Sample 2A: He 1.37, CO_2 : 4.50, Ar: 4.09, N_2 : 3.40) showed good agreement with theoretical Knudsen permselectivity values (He: 1.41, CO_2 : 4.67, Ar: 4.45, N_2 : 3.73), indicating that the pores are controlled finely and homogeneously.

The gas permeation properties through amorphous silica on Samples 1A, 2A, 1B, and 2B at 798 K are shown in Fig. 9. After CDCVD coating, permeance tended to increase with decreasing kinetic diameter. The He and H_2 permeance was not markedly affected by the changes in the pore size and thickness of the γ - Al_2O_3 layer. However, the CO_2 , Ar, and N_2 permeance decreased in the specimens of amorphous silica on Sample 2A and amorphous silica on Sample 2B coated with γ - Al_2O_3 twice. Therefore, the increase in intermediate layer thickness has an effect of decreasing the CO_2 , Ar, and N_2 permeance.

Single gas permeance through amorphous silica on Sample 2B at 373–873 K is shown in Fig. 10. Permeance tended to increase with decreasing kinetic diameter at all permeation temperatures. This membrane showed molecular sieving behavior. The He and H_2 permeance increased with the permeation temperature. On the other hand, the CO_2 , Ar, and N_2 permeance was the lowest at 573 K.

The dependence of temperature on each gas permeance for amorphous silica on Sample 2B is shown in Fig. 11. The He, H_2 , CO_2 , Ar, and N_2 permeance at 798 K was 2.98×10^{-7} , 1.21×10^{-7} , 4.10×10^{-11} , 1.99×10^{-11} , and $9.92 \times 10^{-12} \text{ mol} \cdot (\text{m}^2 \cdot \text{s} \cdot \text{Pa})^{-1}$, respectively. The H_2 permeance at 798 K was four orders of magnitude higher than the N_2 permeance at 798 K, and the H_2/N_2 permselectivity was calculated to be 12200. The He and H_2 permeance increased with the

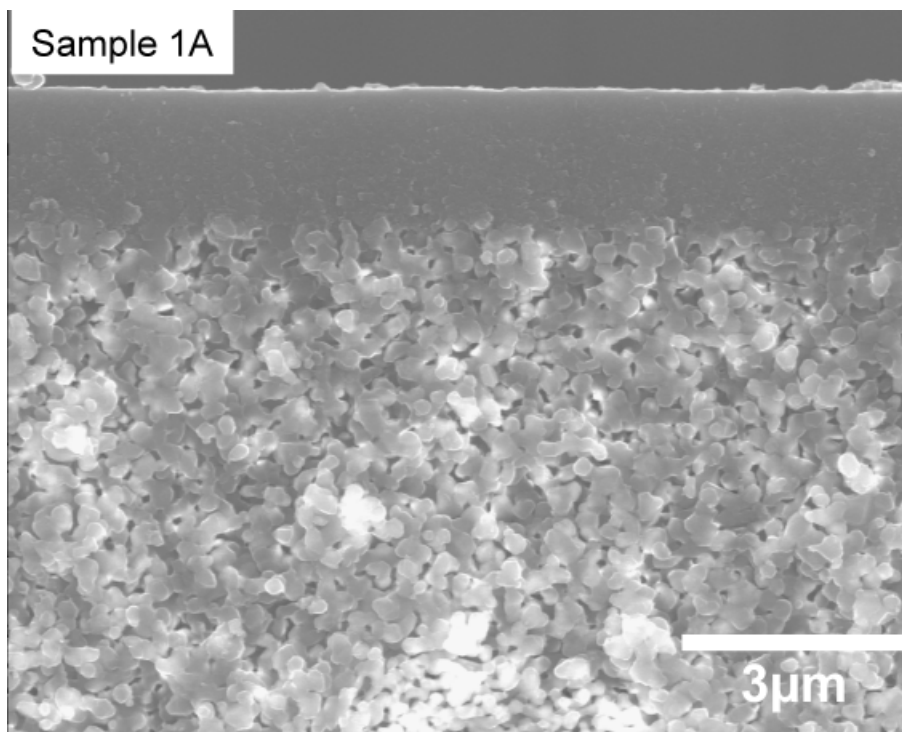


Fig. 5. Scanning electron microscopic cross-sectional image of Sample 1A.

permeation temperature. Accordingly, the dominant permeation mechanism for He and H₂ was considered to be activated diffusion. On the other hand, the CO₂, Ar, and N₂ permeance decreased with increasing permeation temperature at 373–673 K. According to the Knudsen diffusion and viscous flow mechanisms, the permeation of a gas molecule in a porous membrane leads to a decrease in permeance with increasing temperature.

The permeance order of the gases in the Knudsen diffusion mechanism is H₂ > He > N₂ > Ar > CO₂, showing an inverse dependence on the molecular weight of the gases. Therefore, the dominant permeation mechanism for CO₂, Ar, and N₂ was considered to be viscous flow at 373–673 K. These gases were considered to permeate through defects rather than the micropores of the amorphous silica network. However, the CO₂, Ar,

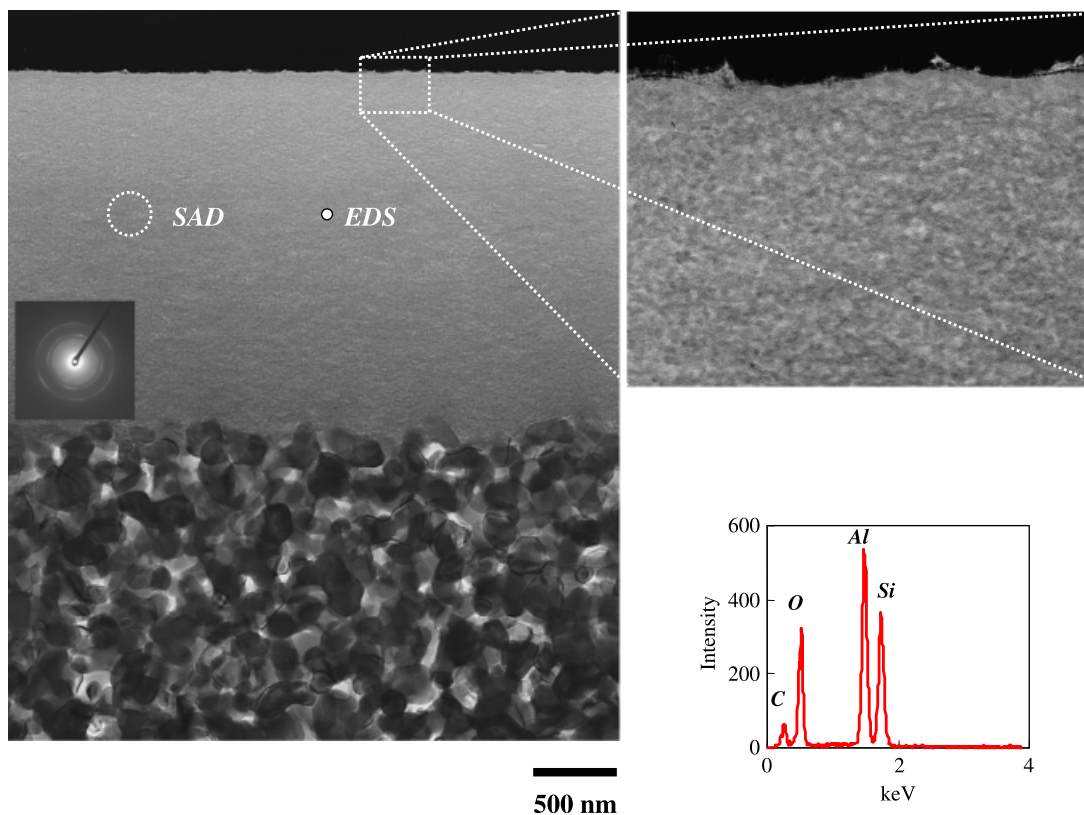


Fig. 6. Transmission electron microscopic cross-sectional images of amorphous silica membrane on Sample 2B.

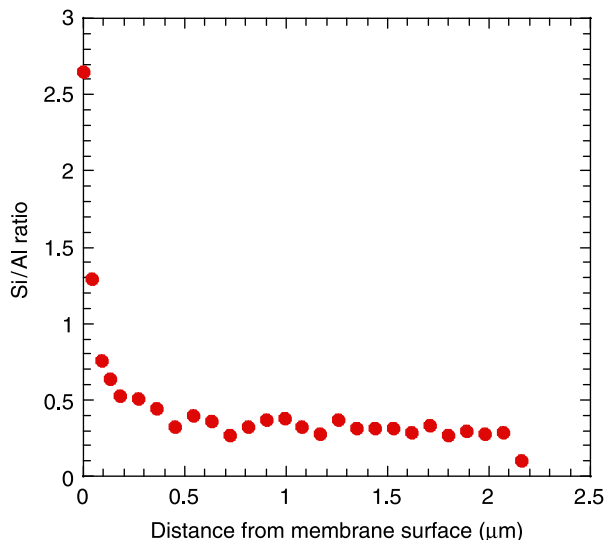


Fig. 7. Distribution of Si/Al ratios for amorphous silica membrane on Sample 2B by energy-dispersive X-ray spectroscopy analysis.

and N₂ permeance increased with the permeation temperature at ≥673 K. This result shows that the dominant permeation mechanism for CO₂, Ar, and N₂ changed to activated diffusion at ≥673 K.

The activation energies of permeation were obtained by fitting the experimental gas permeance data to the Arrhenius expression

$$Q = Q_0 \exp(-E_a/RT) \quad (2)$$

where Q is the permeance, Q_0 the pre-exponential factor ($\text{mol} \cdot (\text{m}^2 \cdot \text{s} \cdot \text{Pa})^{-1}$), E_a the activation energy ($\text{J} \cdot \text{mol}^{-1}$), R the gas constant ($8.314 \text{ J} \cdot (\text{mol} \cdot \text{K})^{-1}$), and T the temperature (K). The apparent activation energies in the amorphous silica membrane on Sample 2B were roughly estimated from the experimental data. The apparent activation energies for the He and H₂ permeance in amorphous silica on Sample 2B were 8.1 and 16.8 kJ/mol in the temperature range from 373 to 873 K, respectively. The apparent activation energy of amorphous silica on Sample 2B for the H₂ permeance was slightly higher than that of amorphous silica on $\gamma\text{-Al}_2\text{O}_3$ -coated $\alpha\text{-Al}_2\text{O}_3$ synthesized by CVD (Hwang *et al.*¹³: 15.3 kJ/mol, Lee *et al.*¹⁸: 14.8 kJ/mol). On the other hand, those for the CO₂, Ar, and N₂ permeance were 26.2,

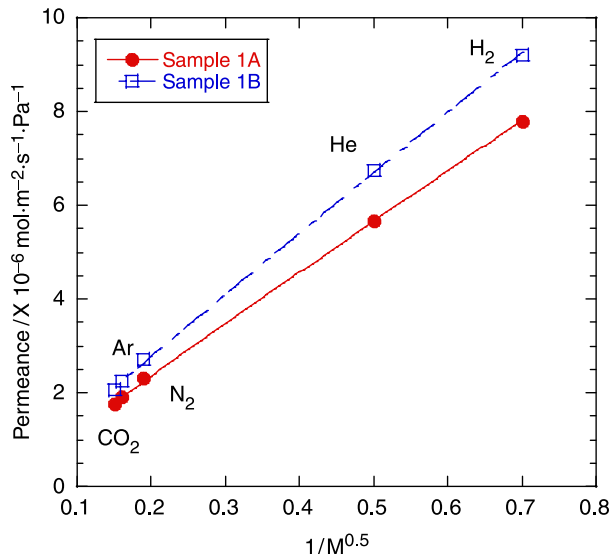


Fig. 8. Gas permeation behavior of Samples 1A and 1B at 873 K.

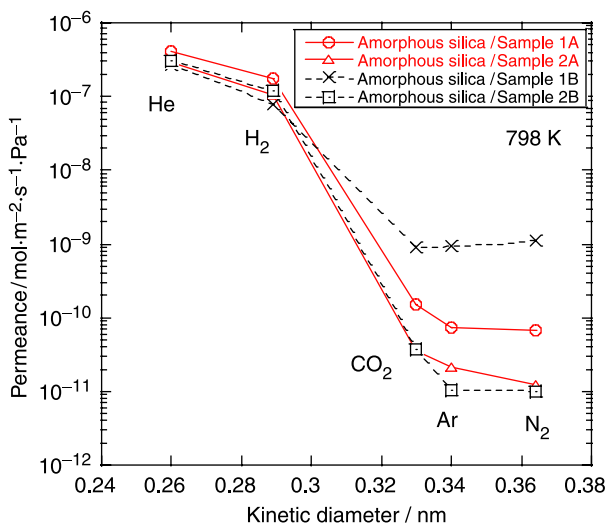


Fig. 9. Effects of number of coatings and pore size on gas permeation behavior.

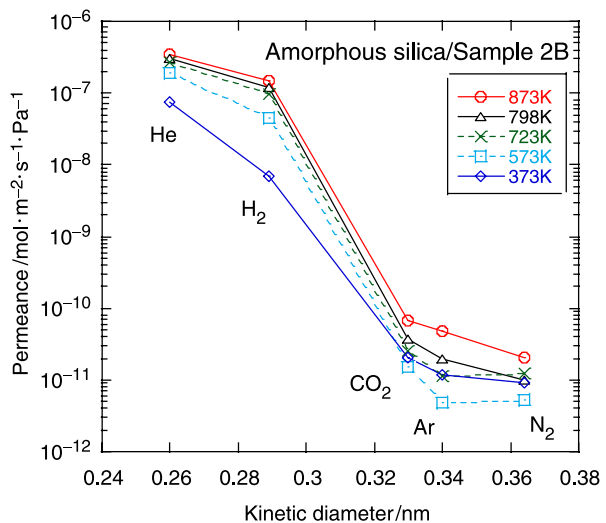


Fig. 10. Gas permeation behavior of amorphous silica on Sample 2B in the temperature range from 373 to 873 K.

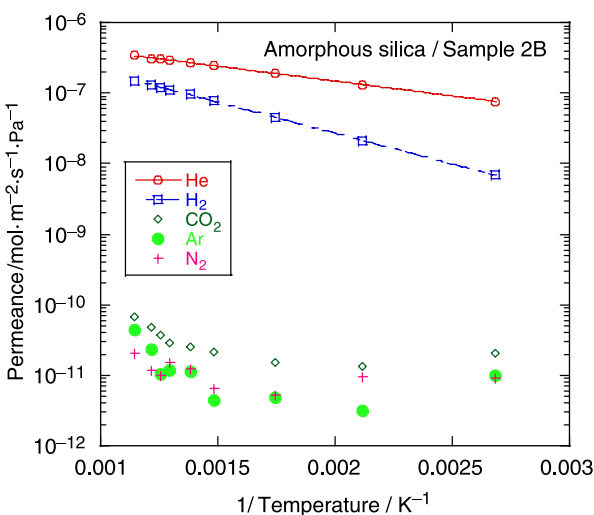


Fig. 11. Dependence of temperature on gas permeance in amorphous silica on Sample 2B.

52.9, and 25.0 kJ/mol in the temperature range from 673 to 873 K, respectively.

As discussed previously, He, H₂, CO₂, Ar, and N₂ through the specimen of amorphous silica on Sample 2B mainly permeated through the amorphous Si–O network at ≥ 673 K. Their permeance depended on the effective area and thickness of the amorphous silica film. Accordingly, the thickness and pore size of the γ -Al₂O₃ intermediate layer are important factors for improving the H₂ permeance to CO₂, Ar, and N₂.

IV. Conclusion

An amorphous silica membrane with molecular-sieving behavior was synthesized on γ -Al₂O₃-coated α -Al₂O₃ by CDCVD. The thickness and pore size distribution of a γ -Al₂O₃ mesoporous intermediate layer were significant factors in H₂ permselectivity. The optimization of the intermediate layer structure is very important for decreasing the permeance of gases with large kinetic diameters.

References

- ¹E. Kikuchi, "Membrane Reactor Application to Hydrogen Production," *Catal. Today*, **56** [1/3] 97–101 (2000).
- ²E. Kikuchi, Y. Nemoto, M. Kajikawa, S. Uemiya, and T. Kojima, "Steam Reforming of Methane in Membrane Reactors: Comparison of Electroless-Plating and CVD Membranes and Catalyst Packing Modes," *Catal. Today*, **56** [1/3] 75–81 (2000).
- ³K. Jarosch and H. I. de Lasa, "Novel Riser Simulator for Methane Reforming Using High Temperature Membranes," *Chem. Eng. Sci.*, **54** [10] 1455–60 (1999).
- ⁴T. Okubo and H. Inoue, "Single Gas Permeation through Porous Glass Modified with Tetraethoxysilane," *AIChE J.*, **35** [5] 845–8 (1989).
- ⁵R. J. R. Uhlhorn, K. Keizer, and A. J. Burggraaf, "Gas Transport and Separation with Ceramic Membranes, Part II: Synthesis and Separation Properties of Microporous Membranes," *J. Membr. Sci.*, **66** [2/3] 271–87 (1992).

- ⁶S. W. Nam and G. R. Gavalas, "Stability of H₂-Permeable SiO₂ Films Formed by Chemical Vapor Deposition," *AIChE Symp. Ser.*, **85** [268] 68–74 (1989).
- ⁷G. R. Gavalas, C. E. Megiris, and S. W. Nam, "Deposition of H₂-Permeable SiO₂ Films," *Chem. Eng. Sci.*, **44** [9] 1829–35 (1989).
- ⁸M. Tsapatsis, S. Kim, S. W. Nam, and G. R. Gavalas, "Synthesis of Hydrogen Permeable SiO₂, TiO₂, Al₂O₃, and B₂O₃ Membranes from the Chloride Precursors," *Ind. Eng. Chem. Res.*, **30** [9] 2152–9 (1991).
- ⁹C. E. Megiris and J. H. E. Glezer, "Synthesis of H₂-Permeable Membranes by Modified Chemical Vapor Deposition, Microstructure and Permeability of SiO₂/C/Vycor Membranes," *Ind. Eng. Chem. Res.*, **31** [5] 1293–9 (1992).
- ¹⁰H. Y. Ha, S. W. Nam, S.-A. Hong, and W. K. Lee, "Chemical Vapor Deposition of Hydrogen-Permeable Silica Films on Porous Glass Supports from Tetraethylorthosilicate," *J. Membr. Sci.*, **85** [3] 279–90 (1993).
- ¹¹S. Yan, H. Maeda, K. Kusakabe, S. Morooka, and Y. Akiyama, "Hydrogen-Permeable SiO₂ Membrane Formed in Pores of Alumina Support Tube by Chemical Vapor Deposition with Tetraethyl Orthosilicate," *Ind. Eng. Chem. Res.*, **33** [9] 2096–101 (1994).
- ¹²A. Nijimeijer, B. J. Bladergroen, and H. Verweij, "Low-Temperature CVD Modification of γ -Alumina Membranes," *Microporous Mesoporous Mater.*, **25** [1/3] 179–84 (1998).
- ¹³G.-J. Hwang, K. Onuki, and S. Shimizu, "Studies on Hydrogen Separation Membrane for IS Process, Membrane Preparation with Porous α -Alumina Tube," *JAERI Res.*, **98-002**, 1–8 (1998).
- ¹⁴M. Nomura, K. Ono, S. Gopalakrishnan, T. Sugawara, and S.-I. Nakao, "Preparation of a Stable Silica Membrane by a Counter Diffusion Chemical Vapor Deposition Method," *J. Membr. Sci.*, **251** [1–2] 151–8 (2005).
- ¹⁵D. Li and S.-T. Hwang, "Preparation and Characterization of Silicon Based Inorganic Membrane for Gas Separation," *J. Membr. Sci.*, **59**, 331–52 (1991).
- ¹⁶Y. Iwamoto, K. Sato, T. Kato, T. Inada, and Y. Kubo, "A Hydrogen-Permeable Amorphous Silica Membrane Derived from Polysilazane," *J. Eur. Ceram. Soc.*, **25** [2–3] 257–64 (2005).
- ¹⁷M. Nomura, S. Gopalakrishnan, H. Aida, T. Sugawara, S.-I. Nakao, S. Yamazaki, Y. Iwamoto, R. Kojima, and A. Nakao, "Investigation of a Hydrothermal Stable Hydrogen Permeable Silica Membrane for a Large Membrane Area Module," *Membrane*, **30** [5] 275–81 (2005).
- ¹⁸D. Lee, L. Zhang, S. Niu, and R. F. Saraf, "Synthesis, Characterization, and Gas Permeation Properties of a Hydrogen Permeable Silica Membrane Supported on Porous Alumina," *J. Membr. Sci.*, **231** [1–2] 117–26 (2004). □